

Unstructured Mesh Generation for the Western North Atlantic Tidal Model Domain

Scott C. Hagen¹, D. Michael Parrish²

¹University of Central Florida, Orlando, FL., U.S.A. shagen@mail.ucf.edu

²University of Central Florida, Orlando, FL., U.S.A. dmp24688@ucf.edu

ABSTRACT

This paper presents an *a posteriori* approach to unstructured mesh generation via a localized truncation error analysis and applies it to the Western North Atlantic Tidal (WNAT) model domain. The WNAT model domain encompasses the Gulf of Mexico, the Caribbean Sea, and the North Atlantic Ocean east to the 60° W meridian. In this paper, we focus on the area surrounding the Bahamas.

A bathymetric data set with fine resolution is employed in separate linear, harmonic simulations of shallow water tidal flow for seven different tidal-forcing constituents. Each set of simulation results is used to perform a truncation error analysis of a linear, harmonic form of the depth-averaged momentum equations for each of the different tidal-forcing frequencies. The process has been built upon successful research aiming to produce unstructured grids for large-scale domains that can be used in the accurate and efficient modeling of shallow water flow. The methodology described herein can also be transferred to other modeling applications.

Keywords: Mesh generation, Localized truncation error analysis, Tidal computations

1. INTRODUCTION

Our recent research has shown that a rigorous analysis of the second- and fourth-order truncation errors from the discretization of a linearized form of the momentum equations can be used to optimally place nodes in one- and two-dimensional (2D) domains for tidal computations (Hagen 1998 and 2001, Hagen, Westerink and Kolar 2000a and 2000b, Hagen, Horstman, and Bennett 2002). The localized truncation error analysis is applied to the actual discretized equations and includes approximations to the variables being simulated and their derivatives. A direct result of this research is the ability to assimilate bathymetric data from large gridded data sets (Hagen 2000).

In this paper we present a twofold expansion of our previous work. First, we apply the localized truncation error analysis to the expansive Western North Atlantic Tidal model domain, which includes the Gulf of Mexico, the Caribbean Sea, and the North Atlantic Ocean east to the 60° W meridian. And second, we go beyond examining only the dominant lunar tide (M_2) and include a total of seven different tidal-forcing constituents in the localized truncation error analysis. What follows are brief

descriptions of the domain, model, and truncation error analysis procedure, the truncation error results for each constituent, and a presentation of node spacing requirements. We conclude with a discussion of the results and future work.

2. DOMAIN AND MODEL FORMULATION

2.1 The Western North Atlantic Tidal (WNAT) model domain

The utility of large computational domains has been demonstrated by previous research (Westerink, Luettich and Muccino 1994, Westerink, et al. 1995). Coastal models with large computational domains allow accurate specification of boundary conditions, since the open boundaries are placed in the deep ocean where flow behavior is linear, and tidal constituents may be more accurately defined. We see deep-water placement of the open boundary as advantageous compared to placement on the continental shelf or at the shelf break, where bathymetry—and therefore the flow field—changes relatively rapidly.

The open ocean boundary of the WNAT model domain coincides with the 60° W meridian, and lies predominantly

in the deep ocean. The coastal boundaries are composed of the South, Central, and North American coastlines. Because of its great size ($8.347 \times 10^6 \text{ km}^2$) and since high resolution is required in coastal regions to adequately represent geometry and tidal flow, we apply to the present model application an unstructured mesh (648,661 elements; 333,701 nodes) so that we may provide high resolution in areas of shallow water, steep bathymetry, and rapidly changing bathymetric gradient, while providing lower, though still adequate, resolution in the deep ocean (Parrish and Hagen 2001).

2.2 Model formulation

Simulations are performed with ADCIRC-2DDI, a two-dimensional depth-integrated hydrodynamic code

(Luettich, Westerink and Scheffner 1992, Westerink et al. 1994). The governing equations solved herein consist of linearized forms of the generalized wave continuity equation (GWCE) and the momentum equations. The 2D GWCE is given by

$$\frac{\partial^2 \eta}{\partial t^2} + \tau_o \frac{\partial \eta}{\partial t} - g \left[\frac{\partial}{\partial x} \left(h \frac{\partial \eta}{\partial x} \right) - \frac{\partial}{\partial y} \left(h \frac{\partial \eta}{\partial y} \right) \right] - (\tau - \tau_o) \left[\frac{\partial}{\partial x} (uh) - \frac{\partial}{\partial y} (vh) \right] = 0 \quad (1)$$

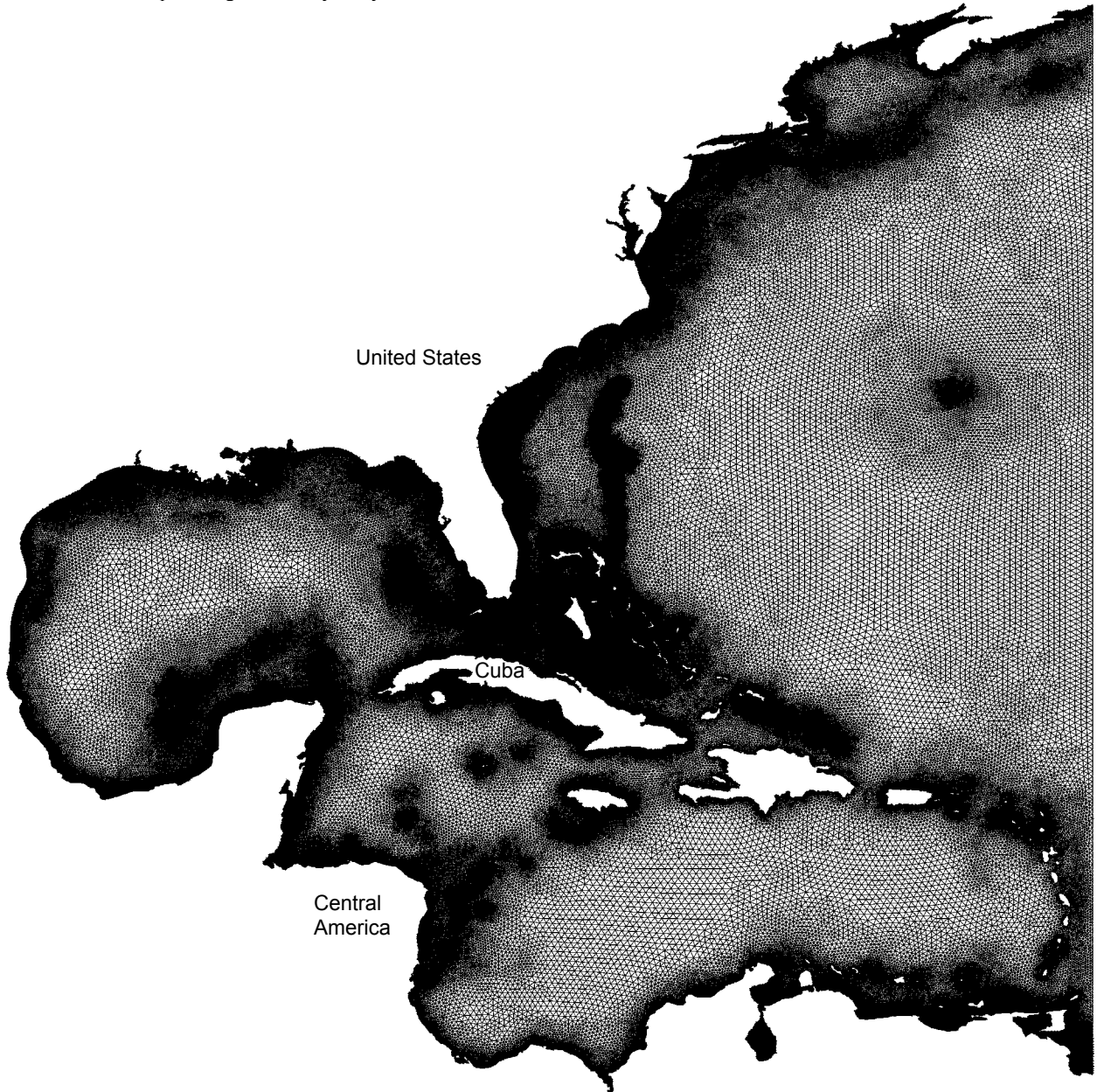


Figure 1. Unstructured mesh for the Western North Atlantic Tidal (WNAT) model domain.

Table 1. Tidal constituents analyzed and the limits of truncation error (TE) estimates.

Constituent (Period in hours)	Minimum TE (m/s ²)	Maximum TE (m/s ²)
M_2 (12.42)	2.37E-14	1.92E-05
N_2 (12.66)	3.24E-15	4.64E-06
S_2 (12.00)	2.29E-14	2.83E-06
K_2 (11.97)	6.26E-15	6.14E-07
K_1 (23.93)	1.90E-14	6.19E-06
O_1 (25.82)	2.50E-14	4.62E-06
Q_1 (26.87)	3.64E-15	8.85E-07

and the 2D, linearized, non-conservative momentum equations are expressed as:

$$\frac{\partial u}{\partial t} + g \frac{\partial \eta}{\partial x} + \tau u = 0 \quad (2)$$

$$\frac{\partial v}{\partial t} + g \frac{\partial \eta}{\partial y} + \tau v = 0 \quad (3)$$

where t = time, x and y = spatial coordinates, η = the deviation of the free surface from the geoid, u = velocity in the x -direction, v = velocity in the y -direction, τ_o = a weighting parameter in the GWCE, which controls the contribution from primitive continuity, g = gravitational acceleration, h = depth below the geoid and τ = the bottom friction coefficient. ADCIRC-2DDI applies linear, Galerkin, triangular finite elements.

The simulations are linear and use a constant bottom friction coefficient of 0.0004 and a GWCE weighting parameter (τ_o) of 0.0004. A no-flow boundary condition is enforced at all land boundaries and open ocean boundaries are depth-forced by a tidal constituent. Fifteen days of real time are simulated to ensure that a dynamic steady-state is achieved. A time step of 20 seconds is used and a hyperbolic ramping function is imposed during the first two days (Luettich, Westerink and Scheffner 1992).

3. LOCALIZED TRUNCATION ERROR ANALYSIS

3.1 Procedure

The truncation error associated with a harmonic form of equations 2 and 3 is developed and estimated for the nodes of an assumed equilateral triangular mesh (Hagen 1998 and 2001, Hagen, Westerink and Kolar 2000b). Sixth- and higher-order terms are truncated and the lower order terms solved for Δ , noting that $\Delta = \Delta_x$ with $\Delta_y = \sqrt{3}\Delta_x$. This permits an estimation of the second and fourth-orders of truncation error associated with the discrete form of

equations 2 and 3 on the interior nodes of an equilateral triangular grid:

$$\begin{aligned} \tau_{ME} = \Delta^2 & \left[\left(\frac{\hat{i}\varpi + \tau}{2} \right) \left(\frac{\partial^2 \hat{u}_k}{\partial x^2} + \frac{\partial^2 \hat{v}_k}{\partial x^2} + \frac{\partial^2 \hat{u}_k}{\partial y^2} + \frac{\partial^2 \hat{v}_k}{\partial y^2} \right) \right. \\ & \left. + \frac{g}{2} \left(\frac{\partial^3 \hat{\eta}_k}{\partial x^3} + \frac{\partial^3 \hat{\eta}_k}{\partial x^2 \partial y} + \frac{\partial^3 \hat{\eta}_k}{\partial x \partial y^2} + \frac{\partial^3 \hat{\eta}_k}{\partial y^3} \right) \right] \\ & + \Delta^4 \left[\left(\frac{\hat{i}\varpi + \tau}{8} \right) \left(\frac{\partial^4 \hat{u}_k}{\partial x^4} + \frac{\partial^4 \hat{v}_k}{\partial x^4} + 2 \frac{\partial^4 \hat{u}_k}{\partial x^2 \partial y^2} \right) \right. \\ & \left. + 2 \left(\frac{\partial^4 \hat{v}_k}{\partial x^2 \partial y^2} + \frac{\partial^4 \hat{u}_k}{\partial y^4} + \frac{\partial^4 \hat{v}_k}{\partial y^4} \right) \right] \\ & + \frac{g}{24} \left[\frac{22}{10} \frac{\partial^5 \hat{\eta}_k}{\partial x^5} + \frac{\partial^5 \hat{\eta}_k}{\partial x^4 \partial y} + 2 \frac{\partial^5 \hat{\eta}_k}{\partial x^3 \partial y^2} \right. \\ & \left. + 6 \frac{\partial^5 \hat{\eta}_k}{\partial x^2 \partial y^3} + 3 \frac{\partial^5 \hat{\eta}_k}{\partial x \partial y^4} + \frac{9}{5} \frac{\partial^5 \hat{\eta}_k}{\partial y^5} \right] \end{aligned} \quad (4)$$

where \hat{u}, \hat{v} and $\hat{\eta}$ are the complex amplitudes of u, v and η evaluated at node k (the center node in the assumed equilateral triangular mesh), g = gravitational acceleration, τ = the bottom friction coefficient, $\hat{i} = \sqrt{-1}$, and ϖ = the response frequency.

3.2 Truncation error for the WNAT model domain

Seven separate simulations using the WNAT mesh (Figure 1) are performed and the individual results are harmonically analyzed from day 12 through day 15 to produce the elevation and x - and y -direction velocity amplitudes and phases. Each simulation is forced at the open ocean boundary by one of seven tidal constituents (Table 1). The localized truncation error is computed for each of the seven constituents by employing central difference approximations with the elevation and velocity amplitudes and phases to estimate the partial derivatives of equation 4 at interior nodes of the WNAT mesh (Hagen 1998 and 2001, Hagen, Westerink and Kolar 2000b). Note that the use of central difference approximations does not permit estimation of truncation error up to and including the boundaries. As a result we are able to estimate truncation error at 215,574 of the 333,701 nodes.

The minimum and maximum truncation error is presented in Table 1. We note that the maximum truncation error is

associated with the M_2 constituent and that this maximum is nearly one order of magnitude larger than all others. The N_2 constituent produces the minimum truncation error and has the largest range at over nine orders of magnitude. The smallest range of truncation error is less than eight orders of magnitude and is associated with the K_2 constituent. There is no clear distinction between semi-diurnal (M_2, N_2, S_2, K_2) and diurnal (K_1, O_1, Q_1) constituents with regards to minimum and maximum error.

The location of the minimum error varies, but it is always located in the deeper regions. Truncation errors are typically lower in the deeper regions and increase in shallower water. For all constituents, the maximum truncation error is found in the same location (see the inset

of Figure 2). On close examination of Figure 2, one can distinguish important bathymetric features (e.g., shelf breaks) highlighted with higher levels of truncation error. Higher truncation errors are exhibited on the shelf regions, with the greatest error found in the Caribbean Sea, north of Cuba and southeast of the Florida peninsula (see the inset of Figure 2). This location of high truncation error indicates a need to provide higher resolution, which will lead to a better description of important topographical features. Truncation error for this region is presented in Figures 3 to 9 and uses the same legend as Figure 2. Figure 3 (M_2 constituent) displays the highest and Figure 6 (K_2 constituent) presents the lowest level of truncation error. These figures indicate that the general distribution of truncation error is similar regardless of forcing constituent.

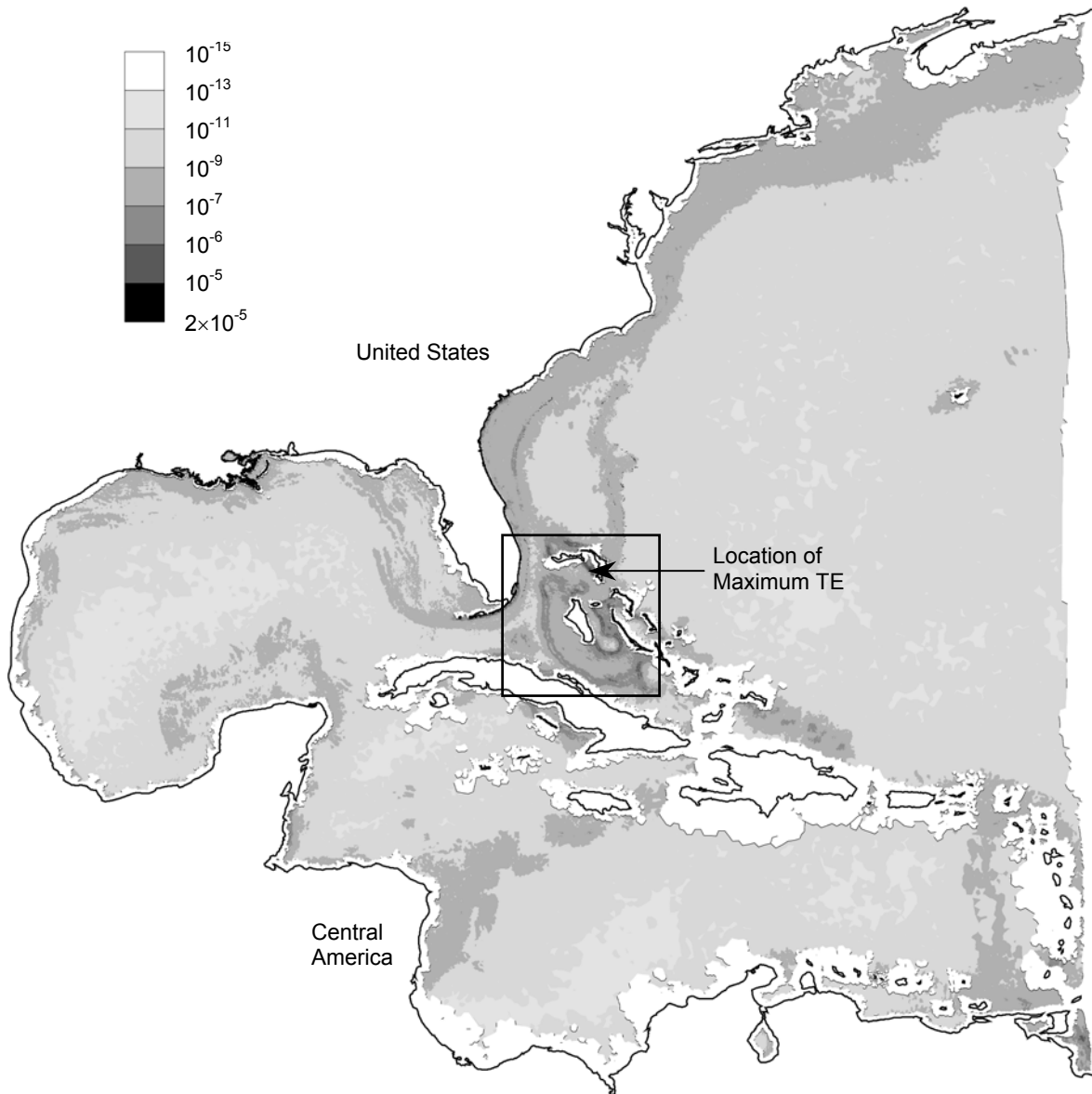


Figure 2. Truncation error contours associated with the M_2 constituent for the WNAT model domain.

3.3 Spacing Requirements for the WNAT Model Domain

In order to determine node spacing requirements as a function of truncation error, equation 4 is set equal to the maximum truncation error and the complex quadratic is solved for Δ . The minimum real root is selected to define spacing requirements (i.e., the minimum allowable node spacing) for interior nodes of the existing finite element mesh (Figure 1). This procedure is carried out for each of the seven separate tidal constituents. Finally, the smallest of the minimum node spacings generated from each of the seven separate tidal constituents is selected at each node.

The node spacing requirements (Figures 10 and 11) that were generated at interior nodes are compared to the mesh sizing used in the existing finite element mesh (Figure 1). On the whole, the existing mesh is more resolved than it needs to be. Only 463 interior nodes were found where the existing spacing exceeds required (i.e., localized truncation error analysis) spacing. There are 431 instances where actual spacing exceeds required spacing by less than 50%; and there are 199 instances where actual spacing exceeds required spacing by less than 10%. Figure 12 displays the few nodes for the inset region that require finer resolution.

We found that for nearly all (99.78% of 215574) of the interior nodes the actual spacing is finer than the required spacing. There are 152,156 instances where the spacing required via truncation error analysis is down to 90% smaller than the required spacing. There are 5309 instances where the actual spacing is down to 50% smaller than the required spacing, and 316 instances where the actual spacing is down to 10% smaller than the required spacing.

In the vicinity of the Bahamas, we found that for nearly all (99.31% of the 34561 nodes enclosed by the inset box) of the interior nodes the actual spacing is finer than the required spacing. There are 26,957 instances where the actual spacing is down to 90% smaller than the required spacing. There are 2957 instances where the actual spacing is down to 50% smaller than the required spacing, and 208 instances where the actual spacing is down to 10% smaller than the required spacing. Figure 13 displays the levels of over-resolution for the inset region.

Figures 14 to 27 and Table 2 assess the constituent dominance in the spacing requirements. Table 2 presents the number of nodes at which a given constituent produced the minimum node spacing. It should be noted that the K_2 forcing produced the majority of these minimum node spacing requirements. Figures 14 to 27 show where each of these constituents dominated the spacing requirements. All constituents contributed to the node spacing requirements at the shelf break north of the Bahamas. This region contains the steepest bathymetric slope (at ~ 6 degrees), which impacts simulation results regardless of the forcing constituents.

4. DISCUSSION AND FUTURE WORK

Tidal modelers have historically focused on the M_2 constituent when developing criteria for mesh generation. With respect to this work involving localized truncation error analysis for multiple tidal constituents it is clear that

Table 2. Occurrence of constituent dominance.

Constituent	Number of Occurrences
M_2	7931
N_2	23003
S_2	18279
K_2	128954
K_1	9482
O_1	12685
Q_1	15240

attention should be paid to all forcing constituents.

In addition, the localized truncation error analysis approach permits *a posteriori* assimilation of large bathymetric data sets by performing a preliminary linear simulation with a fine-resolution mesh that provides high-level detail of the topographical features for the domain. As a result of the preliminary simulation, important bathymetric features can be recognized and integrated into a future unstructured finite element mesh.

Future work will focus on the inclusion of nonlinear bottom friction, Coriolis terms, tidal potential terms and nonlinear interaction of multiple tidal constituents into the localized truncation error-based procedure.



Figure 3. Truncation Error Contours associated with the M_2 tidal constituent for the area southeast of the Florida peninsula (see the inset of Figure 2).

REFERENCES

Hagen, S.C. (1998) Finite element grids based on a localized truncation error analysis. Ph.D. dissertation, Dept. of Civil Eng. and Geo. Sciences, Univ. of Notre Dame, Notre Dame, IN.

Hagen, S.C. (2000) *A posteriori* assimilation of large gridded bathymetric data sets for shallow water modeling,” *Proc. of the 4th Int. Conf. on HydroInformatics*, CD-ROM, Iowa, USA 23-27 July.

Hagen, S.C., Westerink, J.J. and Kolar, R.L. (2000a) One-dimensional finite element grids based on a localized truncation error analysis. *International J for Numerical Methods in Fluids*, **32**, 241-261.

Hagen, S.C., Westerink, J.J. and Kolar, R.L. (2000b) Two-dimensional, unstructured mesh generation for tidal models. *International J for Numerical Methods in Fluids*, **35**, 669-686.

Hagen, S.C. (2001) Estimation of the truncation error for the linearized, shallow water momentum equations, *Engineering With Computers*, **17**, 354-362.

Hagen, S.C., Horstman, O., and Bennett, R.J. (2002) An unstructured mesh generation algorithm for shallow water modeling,” *International J of Computational Fluid Dynamics*, **16**, 83-91.

Luetlich Jr., R.A., Westerink, J.J. and Scheffner, N.W. (1992) ADCIRC: an advanced three-dimensional circulation model for shelves, coasts and estuaries, Report 1, *Technical Report DRP-92-6*, Department of the Army.

Parrish, D.M. and Hagen, S.C. (2001) Development of a tidal constituent database for the St. Johns River Water Management District, Proc. of the 4th Int. Sym. on Ocean Wave Measurement and Analysis, San Francisco, Edge, B.L. (ed.) American Society of Civil Engineers pp. 1605-1614.

Westerink, J.J., Luetlich, R.A., and Muccino, J.C. (1994) Modeling tides in the western North Atlantic using unstructured graded grids, *Tellus*, **46A**, 178-199.

Westerink, J.J., Blain, C.A., Luetlich Jr., R.A. and Scheffner, N.W. (1994) ADCIRC: an advanced three-dimensional circulation model for shelves, coasts and estuaries, Report 2, *Technical Report DRP-92-6*, Department of the Army.

Westerink, J.J., Luetlich, R.A., Blain, C.A. and Hagen, S.C. (1995) Surface elevation and circulation in continental margin waters, in *Finite Element Modeling of Environmental Problems*, Carey, G.F. (ed.) Wiley.

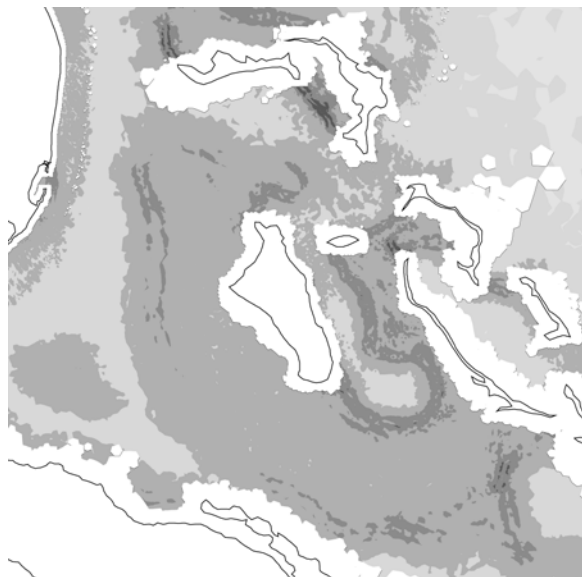


Figure 4. Truncation Error Contours associated with the N_2 tidal constituent for the area southeast of the Florida peninsula (see the inset of Figure 2).

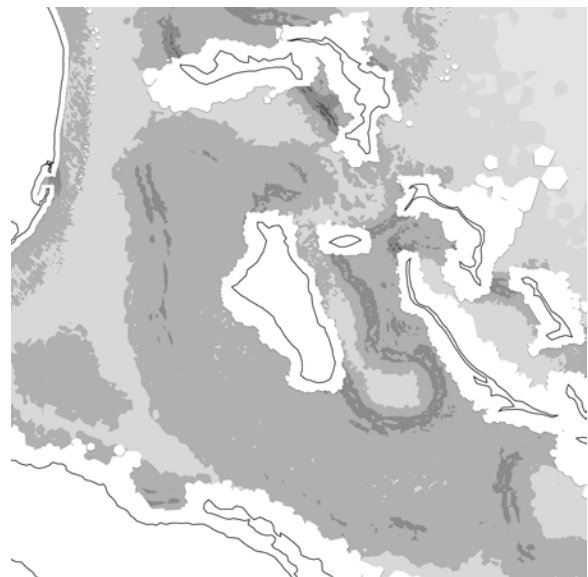


Figure 5. Truncation Error Contours associated with the S_2 tidal constituent for the area southeast of the Florida peninsula (see the inset of Figure 2).



Figure 6. Truncation Error Contours associated with the K_2 tidal constituent for the area southeast of the Florida peninsula (see the inset of Figure 2).

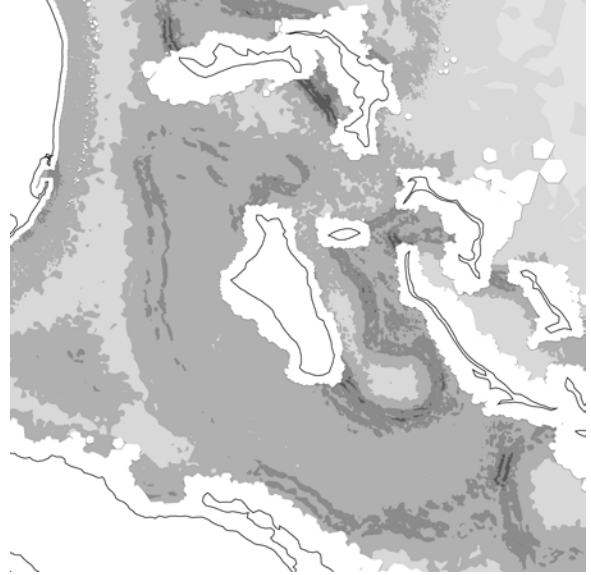


Figure 7. Truncation Error Contours associated with the K_1 tidal constituent for the area southeast of the Florida peninsula (see the inset of Figure 2).

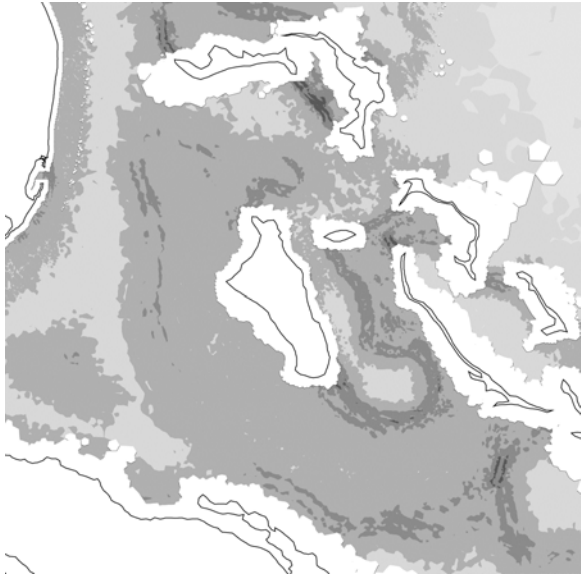


Figure 8. Truncation Error Contours associated with the O_1 tidal constituent for the area southeast of the Florida peninsula (see the inset of Figure 2).

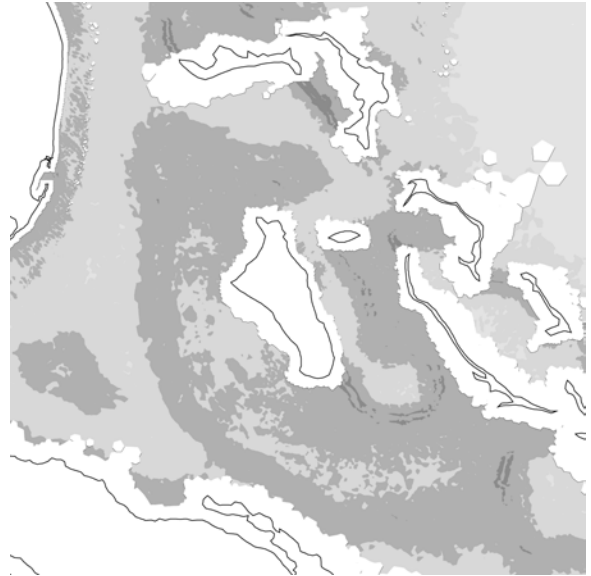


Figure 9. Truncation Error Contours associated with the Q_1 tidal constituent for the area southeast of the Florida peninsula (see the inset of Figure 2).

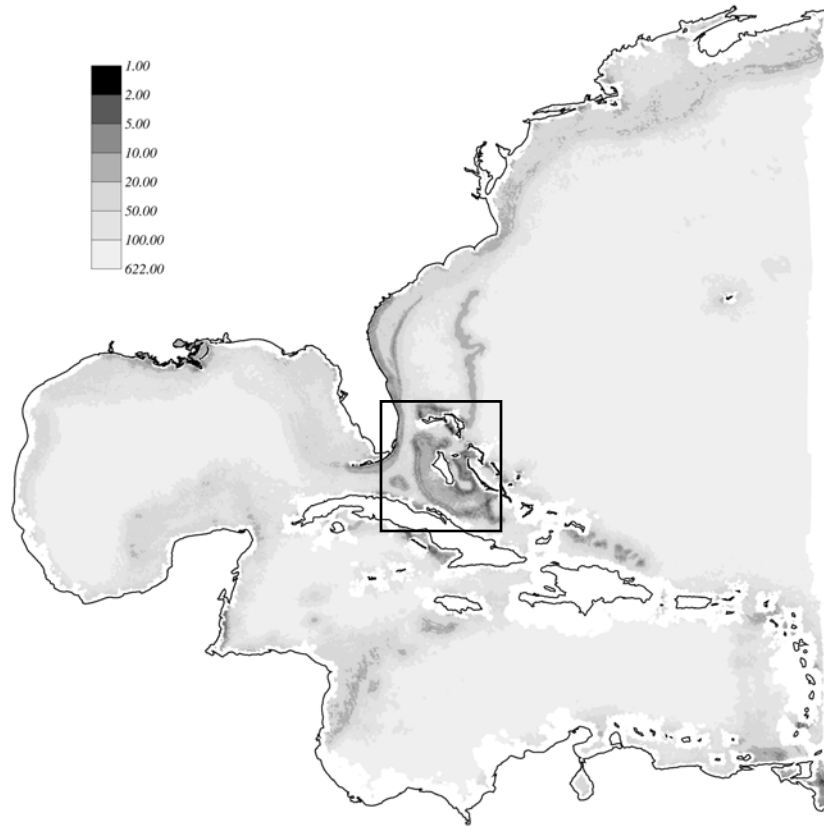


Figure 10. Spacing Requirements in kilometers

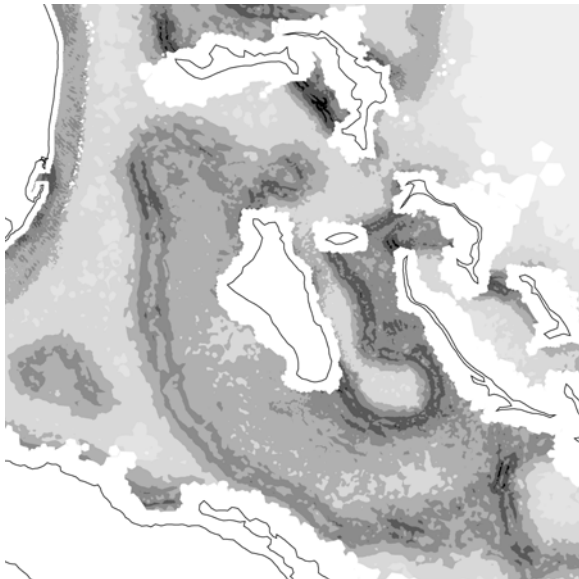


Figure 11. Spacing requirements (detail)



Figure 12. Under-resolved regions (detail)

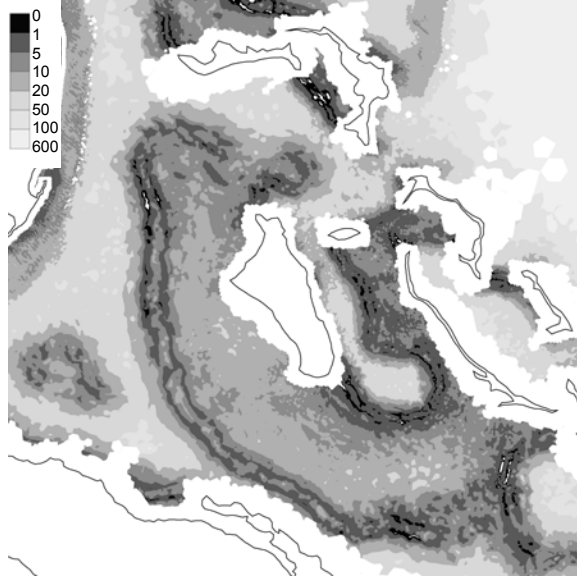


Figure 13. Over-resolved regions (required spacing less actual spacing, km; detail)

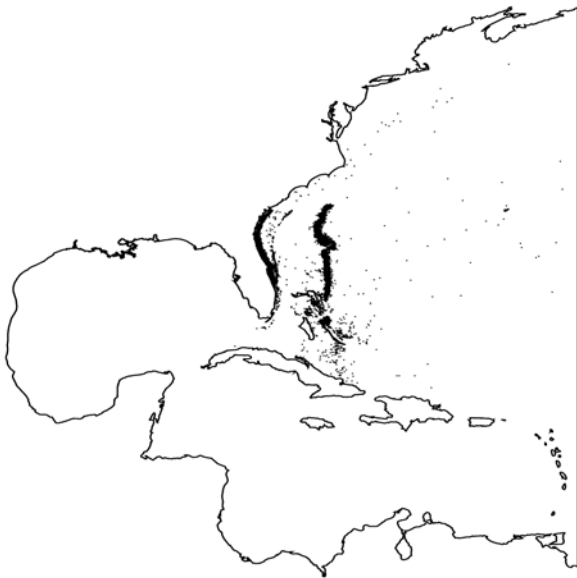


Figure 14. Nodes of M_2 dominance

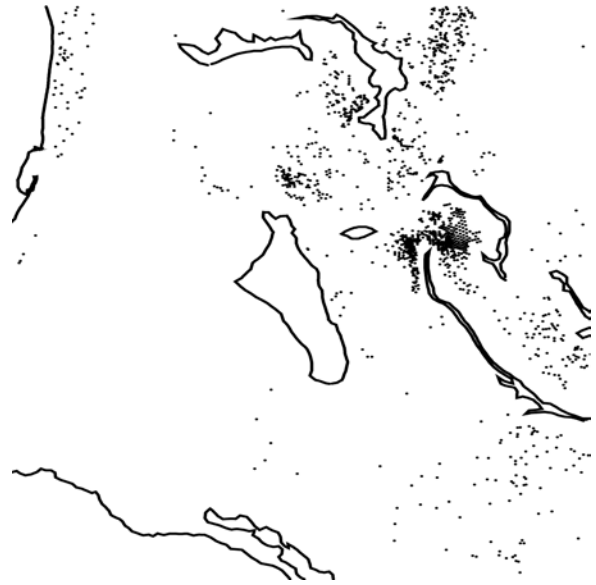


Figure 15. Nodes of M_2 dominance (detail)

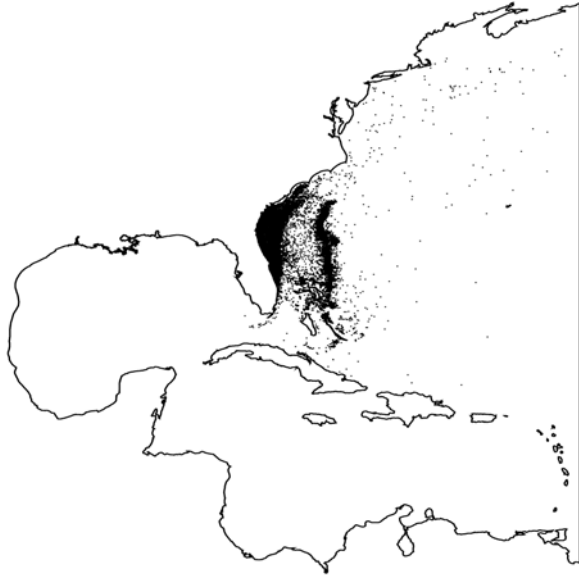


Figure 16. Nodes of N_2 dominance



Figure 17. Nodes of N_2 dominance (detail)

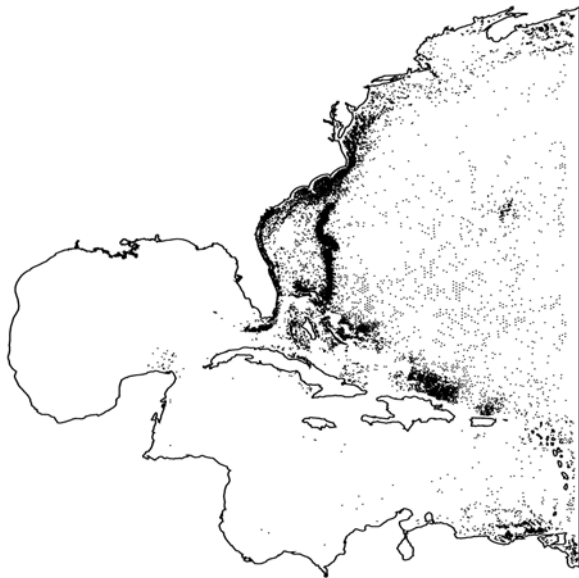


Figure 18. Nodes of S_2 dominance



Figure 19. Nodes of S_2 dominance (detail)

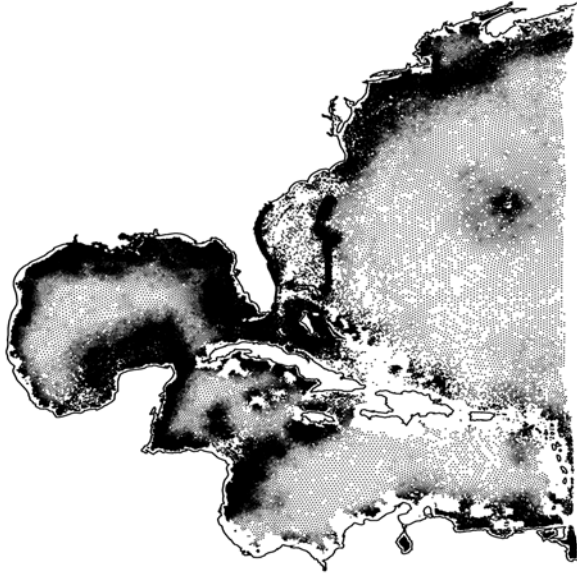


Figure 20. Nodes of K_2 dominance

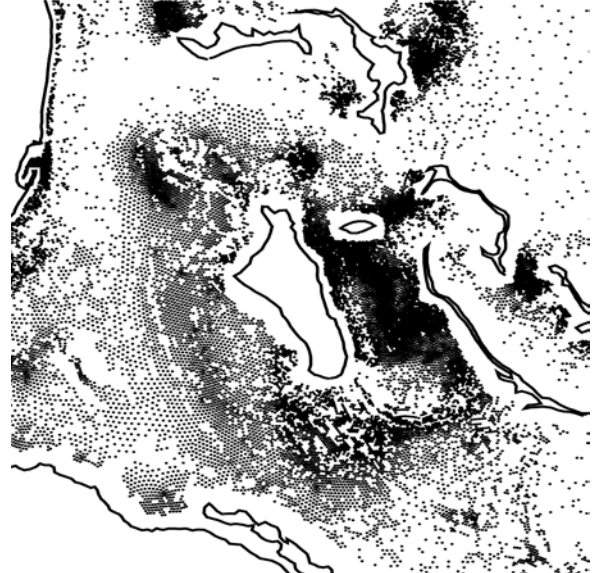


Figure 21. Nodes of K_2 dominance (detail)



Figure 22. Nodes of K_1 dominance



Figure 23. Nodes of K_1 dominance (detail)

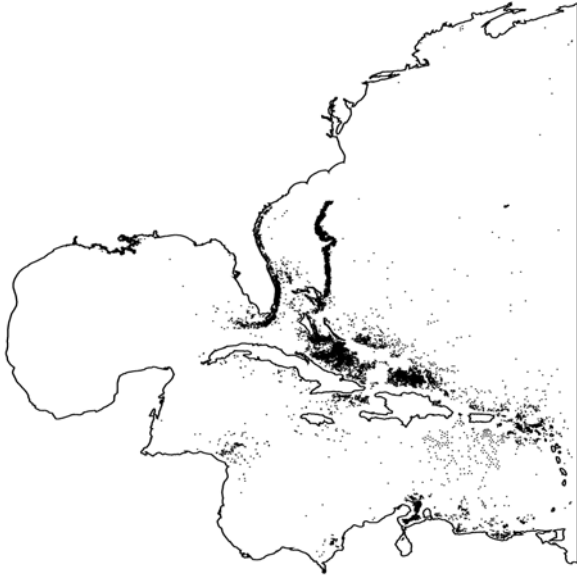


Figure 24. Nodes of O_1 dominance



Figure 25. Nodes of O_1 dominance (detail)

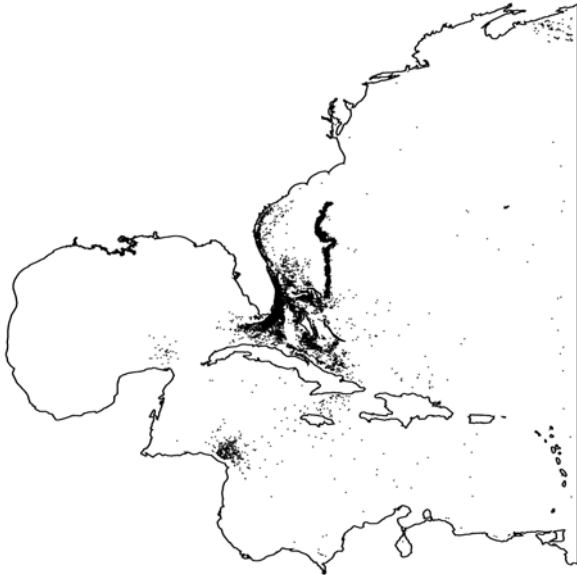


Figure 26. Nodes of Q_1 dominance

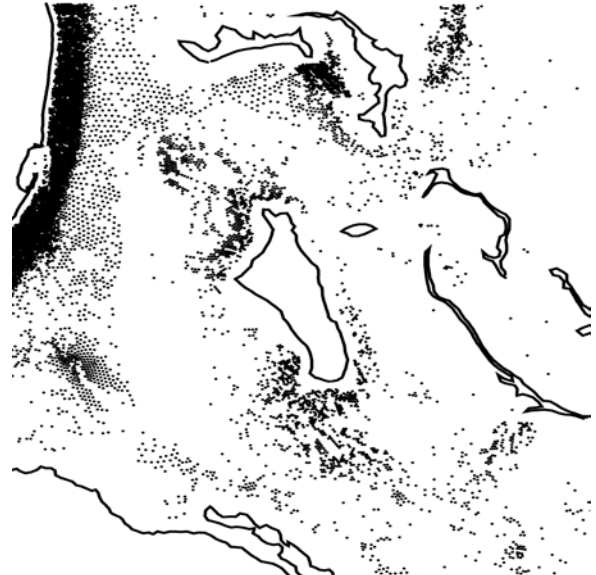


Figure 27. Nodes of Q_1 dominance (detail)